

Comparison of Baseline ^{68}Ga -FAPI and ^{18}F -FDG PET/CT for Prediction of Response and Clinical Outcome in Patients with Unresectable Hepatocellular Carcinoma Treated with PD-1 Inhibitor and Lenvatinib

Meiqi Wu^{*1}, Yanyu Wang^{*2}, Qiao Yang¹, Xuezhu Wang¹, Xu Yang², Haiqun Xing¹, Xinting Sang², Xiang Li³, Haitao Zhao², and Li Huo¹

¹Department of Nuclear Medicine, State Key Laboratory of Complex Severe and Rare Diseases, Center for Rare Diseases Research Beijing Key Laboratory of Molecular Targeted Diagnosis and Therapy in Nuclear Medicine, Peking Union Medical College Hospital, Chinese Academy of Medical Science and Peking Union Medical College, Beijing, China; ²Department of Hepatobiliary Surgery, Peking Union Medical College Hospital, Chinese Academy of Medical Sciences and Peking Union Medical College, Beijing, China; and ³Division of Nuclear Medicine, Department of Biomedical Imaging and Image-Guided Therapy, Medical University of Vienna, Vienna, Austria

Fibroblast activation protein contributes to immunosuppression and resistance to immunotherapies. This study aimed to compare baseline ^{68}Ga -labeled fibroblast activation protein inhibitor (^{68}Ga -FAPI) PET/CT and ^{18}F -FDG PET/CT in response and survival prediction in unresectable hepatocellular carcinoma (uHCC) patients treated with the combination of programmed cell death 1 (PD-1) inhibitor and lenvatinib. **Methods:** In this prospective cohort study, 22 patients with uHCC who underwent baseline ^{18}F -FDG and ^{68}Ga -FAPI PET/CT and soon began taking a combination of PD-1 inhibitor and lenvatinib were recruited. Semiquantitative indices of baseline PET/CT were measured as ^{18}F -FDG SUV_{max} , metabolic tumor volume, total lesion glycolysis, ^{68}Ga -FAPI SUV_{max} , ^{68}Ga -FAPI-avid tumor volume (FTV), and total lesion fibroblast activation protein expression (TLF). The primary endpoint was durable or nondurable clinical benefit after treatment, and the secondary endpoints were progression-free survival (PFS) and overall survival (OS). **Results:** The overall response rate of the combination therapy was 41% (9/22). Fifty percent of patients had durable clinical benefit. Median PFS and OS were 4.8 and 14.4 mo, respectively. Patients with nondurable clinical benefit showed a significantly higher FTV and TLF than those with durable clinical benefit, whereas ^{18}F -FDG parameters overlapped. A higher ^{68}Ga -FAPI-avid tumor burden ($\text{FTV} > 230.46 \text{ cm}^3$ or $\text{TLF} > 961.74 \text{ SUV}_{\text{body weight}} \cdot \text{cm}^3$) predicted both shorter PFS (4.0 vs. 13.5 mo, $P = 0.016$) and shorter OS (7.8 mo vs. not reached, $P = 0.030$). Patients with a higher metabolic tumor burden (metabolic tumor volume $> 206.80 \text{ cm}^3$ or total lesion glycolysis $> 693.53 \text{ SUV}_{\text{body weight}} \cdot \text{cm}^3$) showed a shorter OS although the difference did not reach statistical significance ($P = 0.085$). In multivariate analysis, a higher ^{68}Ga -FAPI-avid tumor burden (hazard ratio [HR], 3.88 [95% CI, 1.26–12.01]; $P = 0.020$) and macrovascular invasion (HR, 4.00 [95% CI, 1.06–15.14]; $P = 0.039$) independently predicted a shorter PFS, whereas a higher ^{68}Ga -FAPI-avid tumor burden (HR, 5.92 [95% CI, 1.19–29.42]; $P = 0.035$) and bone metastases (HR, 5.88 [95% CI, 1.33–25.93]; $P = 0.022$) independently predicted a shorter OS. **Conclusion:** Volumetric indices on baseline ^{68}Ga -FAPI PET/CT were potentially independent

prognostic factors to predict durable clinical benefit, PFS, and OS in uHCC patients treated with a combination of PD-1 and lenvatinib. Baseline ^{68}Ga -FAPI PET/CT may facilitate uHCC patient selection before combination therapy.

Key Words: unresectable hepatocellular carcinoma; PD-1 inhibitor; prognosis; ^{68}Ga -FAPI; PET/CT

J Nucl Med 2023; 64:1532–1539
DOI: 10.2967/jnumed.123.265712

Pharmaceutical advances have changed the therapeutic landscape of unresectable hepatocellular carcinoma (uHCC) (1). In particular, the combination of immune checkpoint blockade (ICB) and multikinase inhibitors has gained remarkable successes in clinical settings (2).

However, only a subportion of patients with uHCC could benefit from ICB therapies (3,4). Reliable predictors for response and patient selection before such combination therapy remained a challenge because of the complexity of the cancer cell metabolism and tumor microenvironment components. Characterization of hepatocellular carcinoma (HCC) by ^{18}F -FDG PET was linked with glycolytic enzymatic activity and differentiation grade, with suboptimal sensitivity in intrahepatic HCC lesions (5). ^{18}F -FDG uptake in HCC and metastasis is significantly associated with recurrence and outcome after curative surgical resection or targeted therapies (6–8). Nevertheless, it is not a reliable marker to predict disease response to systemic therapy.

Tumor microenvironment plays an important role in tumor progression and influences therapeutic response to ICB. Cancer-associated fibroblasts represent the most prominent component of the tumor microenvironment and are composed of different subpopulations exerting distinct functions (9). Fibroblast activation protein (FAP)-positive cancer-associated fibroblasts contribute to immunosuppression in the tumor microenvironment by recruiting inhibitory immune populations such as regulatory T cells and subsets of myeloid cells and are found indicative of primary resistance to immunotherapies (9). In clinical practice, the utility of biomarkers based

Received Mar. 13, 2023; revision accepted May 31, 2023.
For correspondence or reprints, contact Li Huo (huoli@pumch.cn) or Xiang Li (xiang.li@medunwien.ac.at).
^{*}Contributed equally to this work.
Published online Jul. 27, 2023.
COPYRIGHT © 2023 by the Society of Nuclear Medicine and Molecular Imaging.

on tumor tissue is hindered by spatial heterogeneity. PET allows for noninvasive, quantitative, and sensitive whole-body detection of molecular targets. ^{68}Ga -labeled FAP inhibitor (^{68}Ga -FAPI) provided localization and quantification for FAP-positive HCC tumors in our previous studies (10). Particularly, ^{68}Ga -FAPI was superior to ^{18}F -FDG for the detection of primary HCC, allowing improved delineation of whole-body tumor burden (11).

In this prospective study, we aimed to evaluate and compare in vivo tumor metabolism and cancer-associated fibroblast activation using ^{68}Ga -FAPI and ^{18}F -FDG PET/CT for prediction of therapeutic response and survival in uHCC patients treated with a combination of programmed cell death 1 (PD-1) inhibitor and multikinase inhibitor lenvatinib.

MATERIALS AND METHODS

Study Design and Patient Recruitment

This was a prespecified subgroup analysis of a prospective cohort study evaluating the role of ^{68}Ga -FAPI PET/CT in liver and biliary cancer patients and was approved by the Institutional Review Board of Peking Union Medical College Hospital (protocol ZS-1050) and registered at ClinicalTrials.gov (NCT 05662488).

In total, 29 patients with suspected uHCC scheduled to begin receiving PD-1 inhibitor at Peking Union Medical College Hospital were consecutively recruited from July 2020 to April 2022. The diagnosis of uHCC was confirmed by 2 or more experienced hepatobiliary surgeons using the National Comprehensive Cancer Network guidelines. The flowchart of patient enrollment is shown in Figure 1. Clinical, laboratory, and imaging evaluations (contrast-enhanced CT or MRI of the abdomen) were done at enrollment. Previous treatment was recorded. The inclusion criteria were HCC pathologically confirmed or indicated by imaging criteria (12,13); lack of suitability for curative surgery or regional therapy alone, or disease progression after previous therapy; preserved liver function (Child–Pugh class A or B); an Eastern Cooperative Oncology Group performance status score of 0–2; no prior immunotherapy; and no regional therapy within 2 wk.

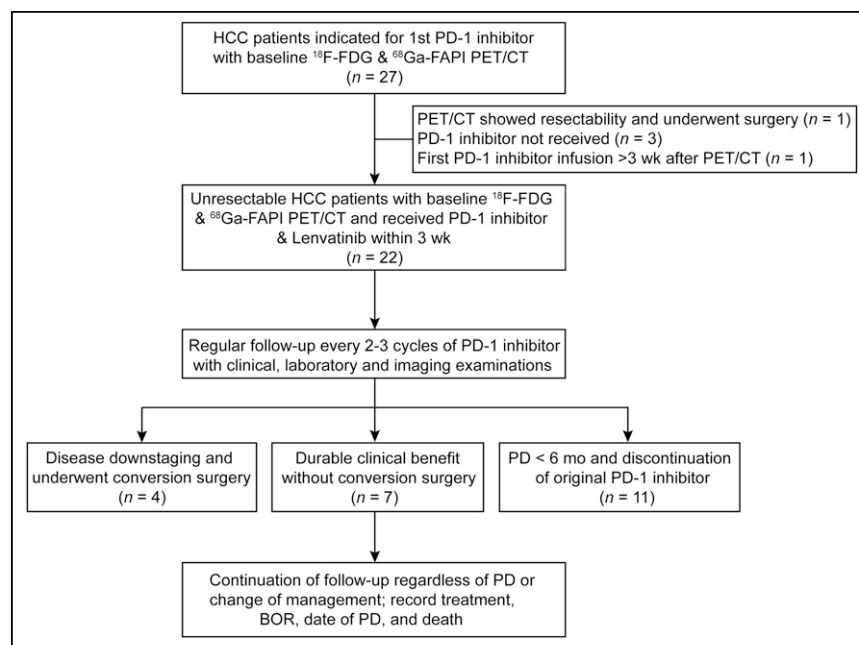


FIGURE 1. Flowchart of patients' enrollment, treatment, and follow-up. BOR = Best objective response.

After enrollment, written informed consent was obtained from each patient. Patients were referred for ^{18}F -FDG and ^{68}Ga -FAPI PET/CT performed no more than 3 d apart. Combination therapy with PD-1 inhibitor (camrelizumab, toripalimab, tislelizumab, or pembrolizumab) and lenvatinib was initiated within 2 wk later. We excluded 7 patients with baseline PET/CT who were later diagnosed with intrahepatic cholangiocarcinoma or combined hepatocellular-cholangiocarcinoma, showed resectability on PET/CT and underwent surgery, did not receive PD-1 inhibitor, or began taking PD-1 inhibitor more than 2 wk after PET/CT. The remaining 22 patients were included in the current study.

PET/CT

The ^{68}Ga -FAPI-04 was radiolabeled manually before injection according to previously published procedures (14). Briefly, ^{68}Ga was chelated after pH adjustment with sodium acetate. The reaction mixture was heated to 100°C for 10 min, and the completeness of the reaction was checked by thin-layer chromatography. ^{18}F -FDG was synthesized in house. All PET/CT scans were performed with a dedicated PET/CT scanner (Polestar m660; SinoUnion) from the tip of the skull to the middle of the thigh (2 min/bed position). Unenhanced low-dose CT scans were obtained for attenuation correction and anatomic positioning. For ^{18}F -FDG PET/CT, the patients fasted for at least 6 h, and blood glucose levels were monitored (<11.0 mmol/L) before injection of ^{18}F -FDG (5.55 MBq/kg). The PET/CT images were acquired with an uptake time of 57–105 min. ^{68}Ga -FAPI PET/CT was performed with an uptake time of 42–90 min after injection (2.22–2.96 MBq/kg). The acquired data were reconstructed using ordered-subset expectation maximization (2 iterations, 10 subsets, gaussian filter, image size of 192×192).

Image Analysis

Two nuclear medicine physicians (both with 4 y of experience in PET/CT reading) reviewed the PET/CT images and recorded focal accumulations not explained by physiologic uptake or inflammation. The physicians were in consensus for image interpretation. Semiquantitative analysis of the PET/CT data was performed on a MIM Workstation (version 6.6.11; MIM Software). The whole-body metabolic tumor burden was measured as metabolic tumor volume (MTV) and total lesion glycolysis (TLG). The whole-body ^{68}Ga -FAPI-avid tumor burden was measured in the same way as the ^{18}F -FDG parameters—as ^{68}Ga -FAPI-avid tumor volume (FTV) and total lesion FAP expression (TLF). A cuboid volume of interest was drawn including all focal lesions in each scan. The tumor contours were semiautomatically segmented with an SUV cutoff of 2.5. The contours were checked and adjusted manually to exclude physiologic or inflammatory uptake. If tracer uptake in the liver with a normal appearance on contrast-enhanced CT or MRI was diffusely elevated and above an SUV of 2.5, a manual contour was applied to enclose hepatic HCC lesions with uptake higher than background. ^{18}F -FDG SUV_{max} , MTV, TLG, ^{68}Ga -FAPI SUV_{max} , FTV, and TLF were automatically generated from the final volumetric extraction.

Follow-up and Clinical Endpoint

All 22 patients were followed up regularly every 2–3 cycles of PD-1 inhibitors (median, 2.1 mo; range, 1.4–3.1 mo) with clinical, laboratory, and imaging examinations (contrast-enhanced CT or MRI). The treatment

response (complete response, partial response, stable disease, or progressive disease) and objective response were evaluated with modified RECIST (15). Durable clinical benefit (DCB) was defined as either the patient's being alive, without next-line systemic treatment and without progressive disease at 6 mo since the first infusion of PD-1 inhibitor, or the patient's experiencing prominent disease downstaging followed by conversion surgery within 6 mo. Nondurable benefit (NDB) was defined as progressive disease or death within 6 mo. Progression-free survival (PFS) and overall survival (OS) were measured from the first PD-1 inhibitor infusion. Treatment regimen, response to therapy, disease progression, and death were recorded. Patients without an event were censored at the time of the last clinical assessment, on December 29, 2022.

Statistical Analysis

The Wilcoxon signed-rank test was applied to test the difference between ^{18}F -FDG and ^{68}Ga -FAPI SUV_{max} , between MTV and FTV, and between TLG and TLF for each patient, whereas the Spearman correlation coefficient was applied to test correlation for each pair. Patients were divided into DCB and NDB groups. The characteristics of the 2 groups were compared using the Fisher exact test for discrete variables and the Student *t* test or Mann-Whitney *U* test for continuous variables. Receiver-operating-characteristic curves were analyzed to estimate the best cutoffs for ^{18}F -FDG SUV_{max} , MTV, TLG, ^{68}Ga -FAPI SUV_{max} , FTV, and TLF between the 2 groups with the maximum Youden index. The Kaplan-Meier method was used to estimate survival curves, which were compared by the log-rank test. Univariable and multivariable analyses using Cox proportional-hazards regression models were performed for PFS and OS. All statistical analyses were done with SPSS (version 25.0; IBM). *P* values of less than 0.05 denoted statistical significance.

RESULTS

Baseline Clinical Characteristics and Dual-Tracer PET Imaging

In total, 22 patients with uHCC who received combination therapy with a PD-1 inhibitor and lenvatinib (19 male and 3 female patients; median age, 62.0 y) were included. Nineteen patients were classified as Barcelona Clinic Liver Cancer stage C. Ten and 5 patients had prior regional or molecular targeted therapy, respectively. All patients had at least 1 lesion with an SUV_{max} above 2.5 on both PET/CT scans. FTV was significantly higher than MTV ($Z = -2.808$, $P = 0.005$), whereas differences between ^{68}Ga -FAPI and ^{18}F -FDG SUV_{max} or between TLG and TLF were not significant. The 3 paired indices all showed medium correlation. The baseline clinical characteristics and PET parameters are summarized in Table 1.

Treatment Efficacy

After baseline assessment, combination therapy with PD-1 inhibitor and lenvatinib began (median interval between PET/CT and initiation of treatment, 4.0 d). Nine, 6, 5, and 2 patients received camrelizumab, toripalimab, tislelizumab, and pembrolizumab, respectively. The choice of PD-1 inhibitor was based on various factors, including the stage of the disease, the line of treatment, individual patient preferences, and the insurance coverage of the drug.

The median duration of follow-up was 16.5 mo (range, 8.0–28.2 mo). All 22 patients had complete radiologic evaluations. During the initial combination therapy, the overall response rate was 41% (9/22): a complete response was achieved in 1 patient, 8 patients had a partial response, 4 patients had stable disease, and 9 patients experienced progressive disease. Eleven (50%) patients had DCB; 4 of them with prominent disease downstaging

TABLE 1
Baseline Characteristics of uHCC Patients ($n = 22$)

Characteristic	Data
Median age (y)	62.0 (range, 35–76)
Age > 65 y	7 (32%)
Sex	
Female	3 (14%)
Male	19 (86%)
Hepatitis B surface antigen A-positive	18 (82%)
Ascites	6 (27%)
Cirrhosis	13 (59%)
ECOG PS	
0 or 1	19 (87%)
2	3 (14%)
Child-Pugh class	
A	15 (68%)
B	7 (32%)
α -fetoprotein > 200 ng/mL	9 (41%)
Macrovascular invasion	16 (73%)
Extrahepatic spread	12 (53%)
Metastases to distant organs	7 (32%)
Bone metastases	3 (14%)
Barcelona Clinic Liver Cancer stage for HCC	
B	3 (14%)
C	19 (86%)
Prior regional treatment	10 (45%)
Partial resection	3 (14%)
Transarterial chemoembolization/radioembolization	8 (36%)
Radiofrequency ablation	2 (9%)
Radiotherapy for bone metastasis	1 (5%)
Prior targeted therapy	5 (23%)
Median ^{18}F -FDG SUV_{max}	6.7 (IQR, 4.5–10.9)
Median MTV (cm^3)	157.4 (IQR, 18.3–365.3)
Median TLG ($\text{SUV}_{\text{bw}} \cdot \text{cm}^3$)	534.8 (IQR, 58.9–1599.5)
Median ^{68}Ga -FAPI SUV_{max}	8.9 (IQR, 6.7–10.9)
Median FTV (cm^3)	312.6 (IQR, 106.4–525.4)
Median TLF ($\text{SUV}_{\text{bw}} \cdot \text{cm}^3$)	1,274.8 (IQR, 323.8–1,840.1)

ECOG PS = Eastern Cooperative Oncology Group performance status; IQR = interquartile range.

Data are number followed by percentage in parentheses, unless indicated otherwise.

underwent conversion surgeries. The other 11 (50%) patients had NDB.

At the time of the analysis, 19 patients discontinued the original combination therapy because of radiologically confirmed

TABLE 2
Comparison of Potential Predictors Between Patients with DCB and NDB

Characteristic	DCB (n = 11)	NDB (n = 11)	P
Age > 65 y	3 (27%)	4 (36%)	1.000
Male	8 (73%)	11 (100%)	0.214
Hepatitis B surface antigen A–positive	8 (73%)	10 (91%)	0.586
Ascites	1 (9%)	5 (45%)	0.149
Cirrhosis	4 (36%)	9 (82%)	0.080
ECOG PS			0.214
0	7 (64%)	4 (36%)	
1	4 (36%)	3 (27%)	
2	0 (0%)	3 (27%)	
Child–Pugh class B	1 (9%)	6 (55%)	0.063
α-fetoprotein > 200 ng/mL	5 (45%)	4 (36%)	1.000
Macrovascular invasion	7 (64%)	9 (82%)	0.635
Extrahepatic spread	6 (55%)	6 (55%)	1.000
Metastases to distant organs	3 (27%)	4 (36%)	1.000
Bone metastases	1 (9%)	2 (18%)	1.000
Barcelona Clinic Liver Cancer stage C	9 (82%)	10 (91%)	1.000
Prior regional treatment	7 (64%)	3 (27%)	0.198
Prior targeted therapy	4 (36%)	1 (9%)	0.311
Median ¹⁸ F-FDG SUV _{max}	5.7 (IQR, 5.0–10.2)	6.9 (IQR, 3.3–13.0)	1.000
Median MTV (cm ³)	154.2 (IQR, 16.1–200.7)	212.9 (IQR, 21.6–463.5)	0.438
Median TLG (SUV _{bw} ·cm ³)	492.2 (IQR, 57.2–693.5)	693.5 (IQR, 62.3–3701.0)	0.365
Median ⁶⁸ Ga-FAPI SUV _{max}	8.8 (IQR, 6.0–10.7)	8.9 (IQR, 8.3–11.5)	0.401
Median FTV (cm ³)	121.3 (IQR, 35.6–337.0)	436.1 (IQR, 289.1–838.9)	0.003
Median TLF (SUV _{bw} ·cm ³)	359.2 (IQR, 120.0–1,344.5)	1,514.3 (IQR, 1,266.8–4,150.3)	0.004

ECOG PS = Eastern Cooperative Oncology Group performance status; IQR = interquartile range.
Data are number followed by percentage in parentheses, unless indicated otherwise.

progressive disease ($n = 15$), intolerable adverse events ($n = 3$), or complete response ($n = 1$). DCB patients tended to receive more cycles of PD-1 inhibitors than NDB patients (median, 12 [interquartile range, 9–14] vs. 3 [interquartile range, 2–5]; $P = 0.13$). Fewer DCB patients than NDB patients experienced progressive disease (7/11 vs. 11/11, $P = 0.09$), with a longer time to progression (13.1 mo [interquartile range, 7.5–15.6 mo] vs. 3.6 mo [interquartile range, 2.8–4.3 mo], $P < 0.01$). Two (18%) patients in the DCB group died after 13.4 and 14.4 mo, respectively. Nine (82%) patients in the NDB group died, with a median OS of 7.3 mo; the follow-up time of the 2 surviving patients was 9.0 and 12.6 mo, respectively. For the entire cohort, the median PFS was 4.8 mo (95% CI, 1.5–8.5 mo) and the median OS was 14.4 mo (95% CI, 12.2–16.6 mo).

Comparison of Imaging and Clinical Factors Between DCB and NDB Groups

Potential predictive factors were compared between patients with DCB and NDB, as shown in Table 2. Patients with DCB had a significantly lower FTV and TLF than patients with NDB ($P < 0.01$). The difference in ¹⁸F-FDG SUV_{max}, MTV, TLG, and

⁶⁸Ga-FAPI SUV_{max} between the 2 groups was not significant. A comparison of the 6 PET indices is shown in Figure 2. Representative baseline ⁶⁸Ga-FAPI and ¹⁸F-FDG PET/CT images of patients with DCB and NDB are shown in Figures 3–5.

More NDB patients than DCB patients had cirrhosis ($P = 0.08$) and Child–Pugh class B ($P = 0.06$), though statistical significance was not reached. No significant difference was found in other clinical factors between patients with DCB and NDB ($P > 0.1$).

To determine the best cutoff of ¹⁸F-FDG SUV_{max}, MTV, TLG, ⁶⁸Ga-FAPI SUV_{max}, FTV, and TLF for survival analyses, receiver-operating-characteristic analysis was performed (Fig. 6). The thresholds selected as the optimal cutoffs for predicting NDB were a TLF of more than 961.74 SUV_{body weight} (SUV_{bw})·cm³ (area under the receiver-operating-characteristic curve [AUC], 0.85; sensitivity, 1.00; specificity, 0.73), an FTV of more than 230.46 cm³ (AUC, 0.86; sensitivity, 1.00; specificity, 0.73), a ⁶⁸Ga-FAPI SUV_{max} of more than 7.04 (AUC, 0.61; sensitivity, 0.91; specificity, 0.45), a TLG of more than 693.53 SUV_{bw}·cm³ (AUC, 0.62; sensitivity, 0.55; specificity, 0.82), an MTV of more than 206.80 cm³ (AUC, 0.60; sensitivity, 0.55; specificity, 0.82), and an ¹⁸F-FDG SUV_{max} of more than 6.69 (AUC, 0.50; sensitivity, 0.63; specificity, 0.64). To note, a TLF of

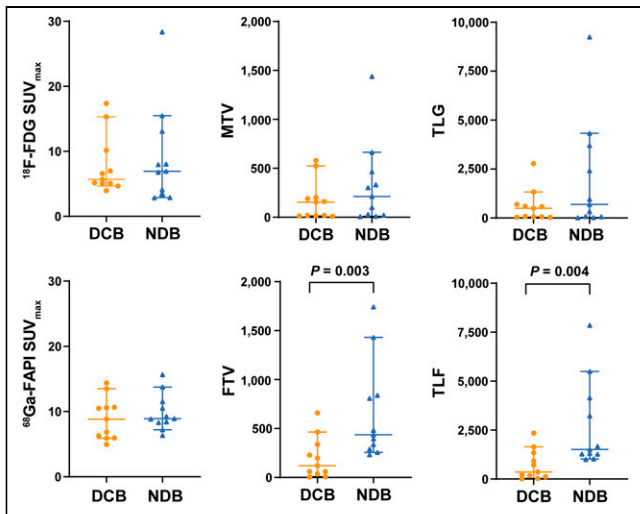


FIGURE 2. Comparison of ^{18}F -FDG SUV_{max} , MTV, and TLG and of ^{68}Ga -FAPI SUV_{max} , FTV, and TLF between DCB and NDB patients.

more than $961.74 \text{ SUV}_{\text{bw}} \cdot \text{cm}^3$ and an FTV of more than 230.46 cm^3 separated the same groups with 14 patients in the higher ^{68}Ga -FAPI-avid tumor burden group and 8 patients in the lower group; a

TLG of more than $693.53 \text{ SUV}_{\text{bw}} \cdot \text{cm}^3$ and an MTV of more than 206.80 cm^3 also separated the same groups with 8 patients in the higher metabolic tumor burden group and 14 in the lower group.

Prognostic Factors for PFS and OS

As shown in Figure 7A, patients with a higher ^{68}Ga -FAPI-avid tumor burden demonstrated a significantly shorter PFS (median PFS, 4.0 mo [95% CI, 3.1–4.8 mo] vs. 13.5 mo [95% CI, 11.5–15.6 mo]; $P = 0.016$). Stratification by ^{18}F -FDG SUV_{max} , MTV/TLG, or ^{68}Ga -FAPI SUV_{max} did not exhibit a different PFS. In univariate analysis, cirrhosis, an Eastern Cooperative Oncology Group performance status of 2, macrovascular invasion, and a higher ^{68}Ga -FAPI-avid tumor burden were significantly associated with poor PFS ($P < 0.1$, Table 3). In multivariate analysis, a higher ^{68}Ga -FAPI-avid tumor burden (hazard ratio [HR], 3.88 [95% CI, 1.26–12.01]; $P = 0.020$) and macrovascular invasion (HR, 4.00 [95% CI, 1.06–15.14]; $P = 0.039$) were significant independent predictors for a shorter PFS.

As shown in Figure 7B, patients with a higher metabolic tumor burden showed a shorter OS, though significance was not reached (median OS, 7.8 mo [95% CI, 5.9–9.6 mo] vs. not reached; $P = 0.085$); patients with a higher ^{68}Ga -FAPI-avid tumor burden showed a significantly shorter OS (median OS, 7.8 mo [95% CI, 5.2–10.4 mo] vs. not reached; $P = 0.030$). In univariate analysis, Child–Pugh B, bone metastases, a higher metabolic tumor burden, and a higher ^{68}Ga -FAPI-avid tumor burden were associated with poor OS ($P < 0.1$, Table 3). In multivariate analysis, bone metastases (HR, 5.88 [95% CI, 1.33–25.93]; $P = 0.022$) and a higher ^{68}Ga -FAPI-avid tumor burden (HR, 5.92 [95% CI, 1.19–29.42]; $P = 0.035$) independently predicted a shorter OS.

DISCUSSION

The ever-growing novel ICB therapies in uHCC have shown distinct efficacies. Therefore, reliable noninvasive biomarkers for response prediction to ICBs are urgently needed to improve patient selection and management. Classic pathologic biomarkers have been evaluated to predict response to PD-1/programmed death ligand 1 inhibitors in HCC patients but have presented contradictory outcomes across studies (1,4). In the current study, we found that the molecular burden of ^{68}Ga -FAPI-avid tumor (FTV and TLF) determined by ^{68}Ga -FAPI PET/CT was strongly associated with a shortened PFS and OS and with NDB in uHCC patients treated with PD-1 inhibitor and lenvatinib. The combination of a high ^{68}Ga -FAPI-avid tumor burden and macrovascular invasion is associated with a shorter PFS, whereas an increased tumor ^{68}Ga -FAPI burden coupled with bone metastases predicted poor OS.

The communication is complicated between tumor metabolism and heterogeneous stromal components in the tumor microenvironment. Previous studies showed that ^{68}Ga -FAPI PET uptake and distribution

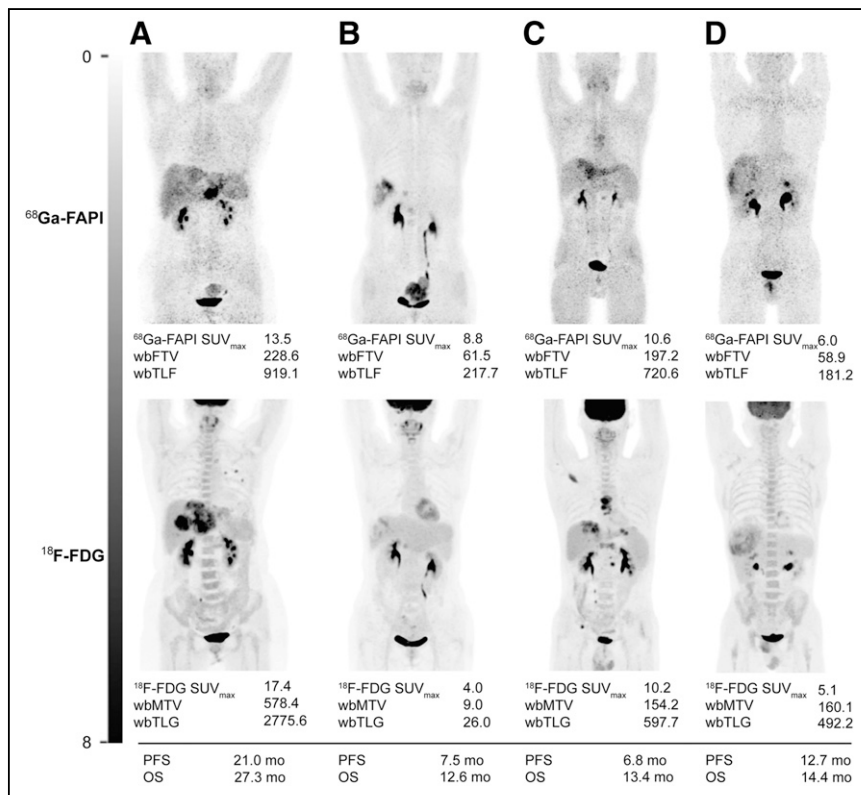


FIGURE 3. Representative baseline ^{68}Ga -FAPI and ^{18}F -FDG PET/CT images of patients with DCB. (A) A 63-y-old woman with multiple hepatic HCC, portal vein invasion, and lung metastases showing low ^{68}Ga -FAPI avidity and high metabolic tumor burden. (B) A 47-y-old woman with right-lobe HCC, portal vein invasion, and lymph node metastases showing low ^{68}Ga -FAPI avidity and metabolic tumor burden. Patients in A and B reached partial response and underwent conversion surgery. (C) A 40-y-old man with multiple intrahepatic lesions, portal vein invasion, lymph node metastases, and bone metastases. (D) A 50-y-old man with right-lobe HCC and portal vein invasion. Patients in C and D had low ^{68}Ga -FAPI avidity and metabolic tumor burden, with stable disease for >6 mo. All 4 patients had OS > 12 mo. wb = whole body.

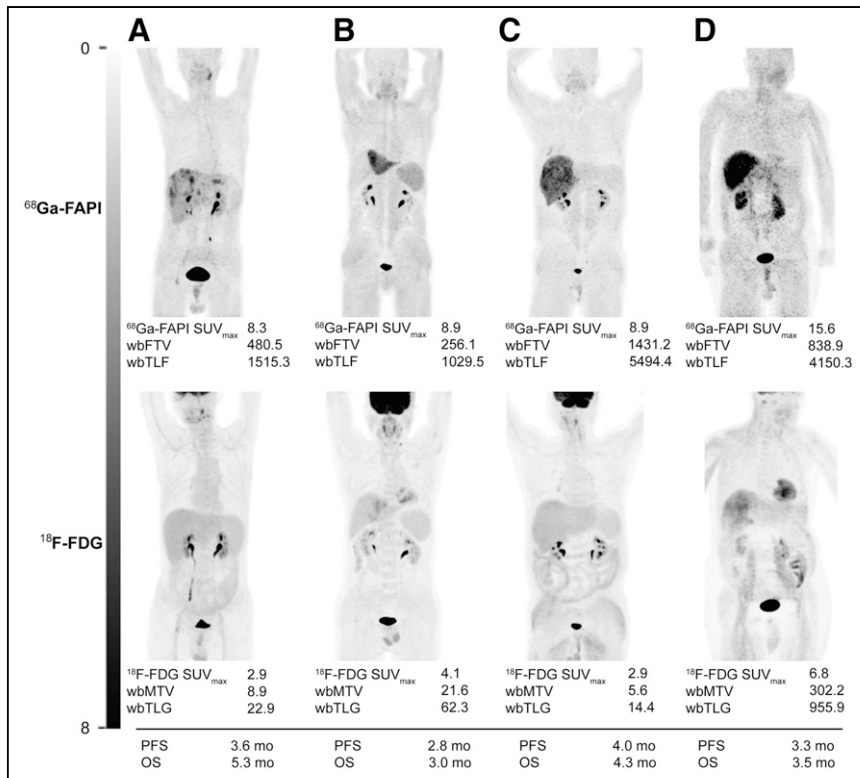


FIGURE 4. Representative baseline $^{68}\text{Ga-FAPI}$ and $^{18}\text{F-FDG}$ PET/CT images of patients with NDB. (A) A 63-y-old man with diffuse HCC. (B) A 69-y-old man with multiple intrahepatic HCC, portal vein invasion, and lung and bone metastases. (C) A 69-y-old man with diffuse right-lobe HCC, portal vein invasion, and lymph node metastases. Patients in A–C showed high $^{68}\text{Ga-FAPI}$ avidity and low metabolic tumor burden. (D) A 71-y-old man with diffuse right-lobe HCC and portal vein invasion showing high $^{68}\text{Ga-FAPI}$ avidity and metabolic tumor burden. All 4 patients progressed on first evaluation after 2–3 cycles of PD-1 inhibitor and had OS of <6 mo. wb = whole body.

strongly correlated with FAP expression characterized by immunohistochemistry in tumor tissues (10,16). FAP-positive cancer-associated fibroblast subsets contribute to immunosuppression through multiple pathways, including assisting differentiation of monocytes to M2-like macrophages, secreting chemokine (C-X-C motif) ligand 12, enhancing recruitment of myeloid-derived suppressor cells, and promoting generation of regulatory T cells (17–20). The current study showcased the potential of $^{68}\text{Ga-FAPI}$ quantification and stromal FAP expression to predict response to ICB in

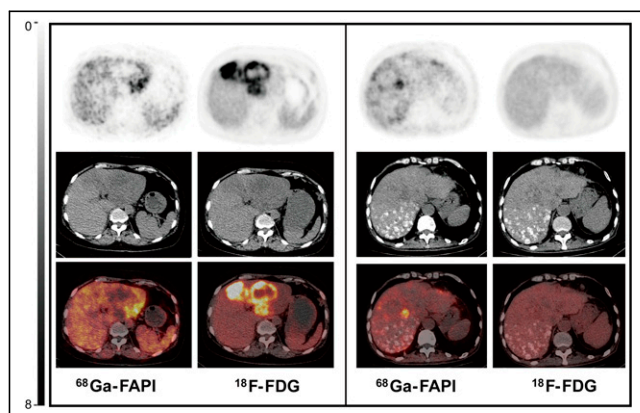


FIGURE 5. Axial PET, CT, and PET/CT images of patients in Figures 3A (left) and 4A (right).

uHCC. The role of FAP-positive cells in HCC immune response is to be further elucidated.

In HCC characterization, $^{18}\text{F-FDG}$ PET/CT is limited by low uptake in well-differentiated HCC and background physiologic activity in the liver. However, a strong correlation between $^{18}\text{F-FDG}$ uptake by primary HCC and tumor differentiation makes $^{18}\text{F-FDG}$ PET/CT valuable in survival prediction. Previous studies found a significant association between pretreatment $^{18}\text{F-FDG}$ uptake or tumor metabolic burden and poor survival in HCC patients treated with transplantation, regional therapy, or targeted therapy (6–8). In this study, we also found that tumor metabolic burden is a prognosticator of OS, extending the prognostic value of $^{18}\text{F-FDG}$ PET in uHCC patients treated with ICB. Importantly, 2 patients (Figs. 4A and 4C) with negligible $^{18}\text{F-FDG}$ -avid lesions and substantial $^{68}\text{Ga-FAPI}$ uptake showed poor survival of less than 6 mo. FTV was higher than MTV in this cohort because more lesions were detected with $^{68}\text{Ga-FAPI}$ PET. The improved sensitivity of intrahepatic lesion detection over $^{18}\text{F-FDG}$ PET can facilitate a better representation of HCC tumor quantification.

The utility of PET/CT in HCC management has been limited. $^{68}\text{Ga-FAPI}$ PET has brought additional value for not merely

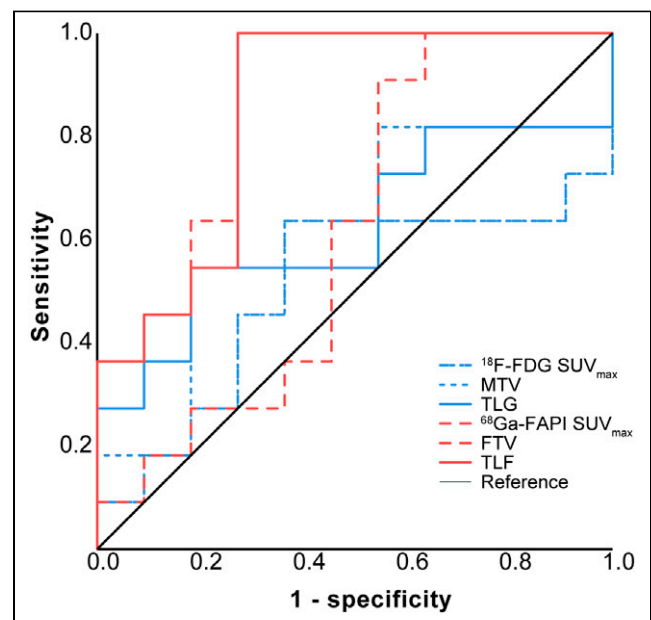


FIGURE 6. Receiver-operating-characteristic analysis curve for $^{18}\text{F-FDG}$ SUV_{max} , TLG, and MTV and for $^{68}\text{Ga-FAPI}$ SUV_{max} , TLF, and FTV for predicting NDB.

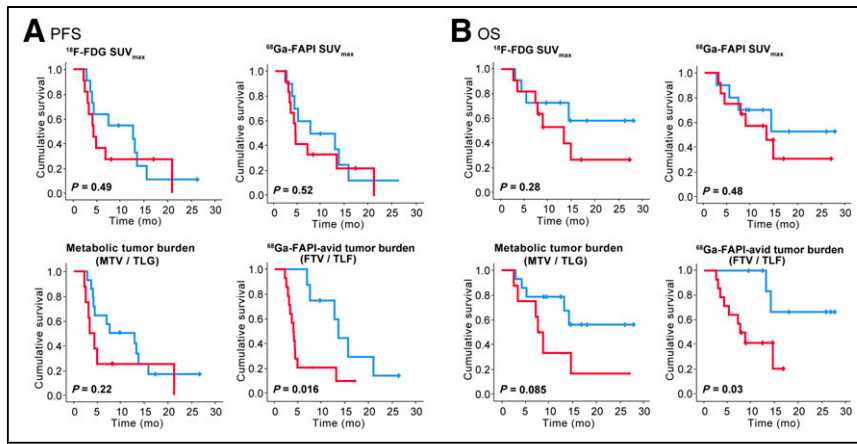


FIGURE 7. Kaplan–Meier curves for PFS (A) and OS (B) in uHCC patients stratified by optimal cutoffs for ^{18}F -FDG SUV_{max} , MTV/TLG, ^{68}Ga -FAPI SUV_{max} , and FTV/TLF.

primary diagnosis, staging, and restaging but also response and survival prediction for HCC, regardless of tumor differentiation. The value of ^{68}Ga -FAPI PET should be further investigated in phase 3 uHCC clinical trials.

of the impact of a single treatment option difficult. The independent value of ^{68}Ga -FAPI PET in patient prognosis should be further investigated in prospective clinical trials. Last, elevated background liver ^{68}Ga -FAPI was found in some patients with

Our study had several limitations. First, the study was limited to a small cohort and different PD-1 regimens. Second, previous treatment for HCC was applied in half the cohort and could potentially have impacted the imaging results and clinical outcomes. Third, regional treatment was incorporated as a combination regimen in some patients. Conversion surgery was applied in 4 patients. The heterogeneous treatment strategies may affect response assessment and outcomes. Only a subset of patients underwent biopsy before combination therapy because of the invasive nature of biopsy. In clinical practice, the sequence of local, regional, and systemic therapies for HCC can significantly differ depending on tumor size and stage and on the patient's condition, making evaluation

TABLE 3
Cox Proportional-Hazards Regression Analysis for PFS and OS

Predictor	PFS				OS			
	Univariable		Multivariable		Univariable		Multivariable	
	HR	P	HR	P	HR	P	HR	P
Age > 65 y	1.01 (0.35–2.91)	0.99			1.85 (0.54–6.41)	0.33		
Male	2.24 (0.50–9.96)	0.29			6.42 (0.23–30.40)	0.36		
HBsAg (+)	1.90 (0.54–6.74)	0.32			2.64 (0.34–20.80)	0.36		
Ascites	1.66 (0.58–4.79)	0.35			2.66 (0.76–9.24)	0.12		
Cirrhosis	2.96 (1.03–8.49)	0.038	2.27 (0.62–8.28)	0.22	1.66 (0.48–5.69)	0.42		
ECOG PS 2	4.34 (1.01–18.6)	0.046	2.83 (0.66–12.21)	0.16	2.91 (0.57–14.72)	0.20		
Child–Pugh class B	1.98 (0.71–5.51)	0.19			3.45 (1.02–11.66)	0.054	1.43 (0.35–5.79)	0.62
AFP > 200 ng/mL	1.46 (0.56–3.74)	0.43			1.27 (0.39–4.19)	0.69		
Macrovascular invasion	3.60 (1.01–12.85)	0.048	4.00 (1.06–15.14)	0.039	2.17 (0.46–10.16)	0.33		
Extrahepatic spread	0.71 (0.27–1.86)	0.49			1.22 (0.37–4.02)	0.75		
Distant-organ metastases	0.93 (0.32–2.66)	0.89			2.07 (0.63–6.83)	0.23		
Bone metastases	2.21 (0.60–8.21)	0.24			4.27 (1.05–17.25)	0.037	5.88 (1.33–25.93)	0.022
BCLC stage C	1.48 (0.34–6.49)	0.61			1.63 (0.21–12.78)	0.64		
Prior regional treatment	0.58 (0.23–1.50)	0.26			0.74 (0.22–2.42)	0.61		
Prior targeted therapy	0.39 (0.11–1.37)	0.14			0.25 (0.03–1.96)	0.19		
^{18}F -FDG $\text{SUV}_{\text{max}} > 6.69$	1.39 (0.55–3.52)	0.49			1.94 (0.57–6.66)	0.29		
MTV > 206.80 cm^3 or TLG > 693.53 $\text{SUV}_{\text{bw}} \cdot \text{cm}^3$	1.81 (0.69–4.76)	0.23			2.74 (0.83–9.07)	0.10	2.80 (0.83–9.42)	0.10
^{68}Ga -FAPI $\text{SUV}_{\text{max}} > 7.04$	1.36 (0.53–3.45)	0.52			1.55 (0.45–5.30)	0.49		
FTV > 230.46 cm^3 or TLF > 961.74 $\text{SUV}_{\text{bw}} \cdot \text{cm}^3$	3.54 (1.20–10.45)	0.015	3.88 (1.26–12.01)	0.020	4.83 (1.02–22.88)	0.048	5.92 (1.19–29.42)	0.035

HBsAg (+) = hepatitis B surface antigen A-positive; ECOG PS = Eastern Cooperative Oncology Group performance status; AFP = α -fetoprotein; BCLC = Barcelona Clinic Liver Cancer.

Data in parentheses are 95% CIs.

cirrhosis, and manual contours were carefully applied. The value of cirrhosis-mediated FAP activity in HCC prognosis warrants further investigation (21).

CONCLUSION

Volumetric indices on baseline ^{68}Ga -FAPI PET/CT were potentially independent prognostic factors to predict DCB, PFS, and OS in uHCC patients treated with a combination of PD-1 inhibitor and lenvatinib. Baseline ^{68}Ga -FAPI PET/CT may facilitate selection of uHCC patients for the combination of ICB and targeted therapy.

DISCLOSURE

This work was sponsored in part by the National Natural Science Foundation of China (82071967), the CAMS innovation fund for medical science (CIFMS-2021-I2 M-1-025, CIFMS-2021-I2 M-1-002, CIFMS-2021-I2 M-1-061, and CIFMS-2022-I2 M-C&T-A-003), and National High Level Hospital Clinical Research Funding (2022-PUMCH-B-070). No other potential conflict of interest relevant to this article was reported.

KEY POINTS

QUESTION: Can baseline ^{68}Ga -FAPI PET predict response and survival in uHCC patients treated with ICB-based combination therapy?

PERTINENT FINDINGS: Volumetric indices on baseline ^{68}Ga -FAPI PET/CT can potentially predict DCB, PFS, and OS in uHCC patients treated with a combination of PD-1 inhibitor and lenvatinib.

IMPLICATIONS FOR PATIENT CARE: Baseline ^{68}Ga -FAPI PET/CT may facilitate uHCC patient selection for the combination of ICB and targeted therapy.

REFERENCES

1. Yang C, Zhang H, Zhang L, et al. Evolving therapeutic landscape of advanced hepatocellular carcinoma. *Nat Rev Gastroenterol Hepatol*. 2023;20:203–222.
2. Reig M, Forner A, Rimola J, et al. BCLC strategy for prognosis prediction and treatment recommendation: the 2022 update. *J Hepatol*. 2022;76:681–693.
3. Cheng AL, Hsu C, Chan SL, Choo SP, Kudo M. Challenges of combination therapy with immune checkpoint inhibitors for hepatocellular carcinoma. *J Hepatol*. 2020;72:307–319.
4. Yau T, Park JW, Finn RS, et al. Nivolumab versus sorafenib in advanced hepatocellular carcinoma (CheckMate 459): a randomised, multicentre, open-label, phase 3 trial. *Lancet Oncol*. 2022;23:77–90.
5. Asman Y, Evenson AR, Even-Sapir E, Shibolet O. [^{18}F]fludeoxyglucose positron emission tomography and computed tomography as a prognostic tool before liver transplantation, resection, and loco-ablative therapies for hepatocellular carcinoma. *Liver Transpl*. 2015;21:572–580.
6. Lee JW, Oh JK, Chung YA, et al. Prognostic significance of ^{18}F -FDG uptake in hepatocellular carcinoma treated with transarterial chemoembolization or concurrent chemoradiotherapy: a multicenter retrospective cohort study. *J Nucl Med*. 2016;57:509–516.
7. Na SJ, Oh JK, Hyun SH, et al. ^{18}F -FDG PET/CT can predict survival of advanced hepatocellular carcinoma patients: a multicenter retrospective cohort study. *J Nucl Med*. 2017;58:730–736.
8. Sung PS, Park HL, Yang K, et al. ^{18}F -fluorodeoxyglucose uptake of hepatocellular carcinoma as a prognostic predictor in patients with sorafenib treatment. *Eur J Nucl Med Mol Imaging*. 2018;45:384–391.
9. Peltier A, Seban RD, Buvat I, Bidard FC, Mehta-Grigoriou F. Fibroblast heterogeneity in solid tumors: from single cell analysis to whole-body imaging. *Semin Cancer Biol*. 2022;86:262–272.
10. Shi X, Xing H, Yang X, et al. Fibroblast imaging of hepatic carcinoma with ^{68}Ga -FAPI-04 PET/CT: a pilot study in patients with suspected hepatic nodules. *Eur J Nucl Med Mol Imaging*. 2021;48:196–203.
11. Shi X, Xing H, Yang X, et al. Comparison of PET imaging of activated fibroblasts and ^{18}F -FDG for diagnosis of primary hepatic tumours: a prospective pilot study. *Eur J Nucl Med Mol Imaging*. 2021;48:1593–1603.
12. Heimbach JK, Kulik LM, Finn RS, et al. AASLD guidelines for the treatment of hepatocellular carcinoma. *Hepatology*. 2018;67:358–380.
13. Zhou J, Sun HC, Wang Z, et al. Guidelines for diagnosis and treatment of primary liver cancer in China (2017 edition). *Liver Cancer*. 2018;7:235–260.
14. Lindner T, Loktev A, Altmann A, et al. Development of quinoline-based theranostic ligands for the targeting of fibroblast activation protein. *J Nucl Med*. 2018;59:1415–1422.
15. Lencioni R, Llovet JM. Modified RECIST (mRECIST) assessment for hepatocellular carcinoma. *Semin Liver Dis*. 2010;30:52–60.
16. Hirnas N, Hamacher R, Sraieb M, et al. Fibroblast-activation protein PET and histopathology in a single-center database of 324 patients and 21 tumor entities. *J Nucl Med*. 2023;64:711–716.
17. Kraman M, Bambrough PJ, Arnold JN, et al. Suppression of antitumor immunity by stromal cells expressing fibroblast activation protein- α . *Science*. 2010;330:827–830.
18. Feig C, Jones JO, Kraman M, et al. Targeting CXCL12 from FAP-expressing carcinoma-associated fibroblasts synergizes with anti-PD-L1 immunotherapy in pancreatic cancer. *Proc Natl Acad Sci USA*. 2013;110:20212–20217.
19. Fearon DT. The carcinoma-associated fibroblast expressing fibroblast activation protein and escape from immune surveillance. *Cancer Immunol Res*. 2014;2:187–193.
20. Lakins MA, Ghorani E, Munir H, Martins CP, Shields JD. Cancer-associated fibroblasts induce antigen-specific deletion of CD8 (+) T cells to protect tumour cells. *Nat Commun*. 2018;9:948.
21. Pirasteh A, Periyasamy S, Meudt JJ, et al. Staging liver fibrosis by fibroblast activation protein inhibitor PET in a human-sized swine model. *J Nucl Med*. 2022;63:1956–1961.